ARTICLES
PUBLISHED ONLINE: 31 AUGUST 2014 | DOI: 10.1038/NPHOTON.2014.189
nature photonics

Non-invasive single-shot imaging through scattering layers and around corners via speckle correlations

Ori Katz[1,2]*, Pierre Heidmann[1], Mathias Fink[1] and Sylvain Gigan[1,2]

Optical imaging through and inside complex samples is a difficult challenge with important applications in many fields. The fundamental problem is that inhomogeneous samples such as biological tissue randomly scatter and diffuse light, preventing the formation of diffraction-limited images. Despite many recent advances, no current method can perform non-invasive imaging in real-time using diffused light. Here, we show that, owing to the 'memory-effect' for speckle correlations, a single high-resolution image of the scattered light, captured with a standard camera, encodes sufficient information to image through visually opaque layers and around corners with diffraction-limited resolution. We experimentally demonstrate single-shot imaging through scattering media and around corners using spatially incoherent light and various samples, from white paint to dynamic biological samples. Our single-shot lensless technique is simple, does not require wavefront-shaping nor time-gated or interferometric detection, and is realized here using a camera-phone. It has the potential to enable imaging in currently inaccessible scenarios.

Diffraction-limited optical imaging is an indispensable tool in many fields of research. Unfortunately, however, the inherent inhomogeneity of complex samples such as biological tissues induces light scattering, which diffuses any optical beam into a complex speckle pattern[1], limiting the resolution and penetration depth of optical imaging techniques[2]. Many approaches to overcome this fundamental, yet practical, problem have been put forward over the years, with pioneering experiments in holography dating back to just a few years after the invention of the laser[3,4]. However, to date, no approach allows real-time non-invasive imaging using diffused light. Modern techniques that are based on using only unscattered, 'ballistic' light, such as optical coherence tomography and two-photon microscopy, have proven very useful, but are inherently limited to shallow depths where a measurable amount of unscattered photons is present. Adaptive optics techniques[5] can near-perfectly correct low-order aberrations using deformable mirrors, but require the presence of a bright point-source 'guide star' or a high initial image contrast[6]. Recent exciting advances in controlled wavefront shaping[7] have allowed focusing and imaging through highly scattering samples[8–26]. However, these techniques either require initial access to both sides of the scattering medium[8–15], the presence of a guide-star or a known object[16–19], or a long acquisition sequence that involves the projection of a large number of optical patterns[20–26]. A recent breakthrough approach reported by Bertolotti *et al.* has removed the requirement for a guide-star or a prior calibration sequence by exploiting the inherent angular correlations in scattered speckle patterns, which are scanned over the target object[27]. However, the requirement for a set of high-resolution angular scans of a coherent laser beam[27,28] restricts this approach to objects and scattering samples that remain completely stationary over the long acquisition sequence.

Here, we present a technique that allows the non-invasive imaging of hidden objects through visually opaque layers and around corners in real time, using spatially incoherent light and a standard digital camera (Fig. 1a–d). We show that a single image of the scattered light that diffuses through a scattering medium encodes sufficient information to image through it, with diffraction-limited resolution. Specifically, derived from concepts used in 'stellar speckle interferometry'[29–31] and the angular 'memory-effect' for speckle correlations[32–34] exploited in Bertolotti's technique[27], we show that the autocorrelation of the scattered light pattern (Fig. 1c) is essentially identical to the autocorrelation of the object's image itself (Fig. 1g). We then reconstruct the object's image from its autocorrelation using an iterative Fienup-type algorithm[35]. As proofs of concept, we experimentally demonstrate our single-shot non-invasive technique through a variety of highly scattering samples, from optical diffusers to dynamically varying biological tissues. In addition, we demonstrate imaging 'around corners' by recording the diffuse light back-scattered off white-painted 'walls'.

Principle

A schematic of the experiment for imaging through a scattering medium, as well as a numerical example, are presented in Fig. 1a–d. An object is hidden at a distance u behind a highly scattering medium of thickness L. The object is illuminated by a spatially incoherent, narrowband source, and a high-resolution camera that is placed at a distance v on the other side of the medium records the pattern of the scattered light that has diffused through the scattering medium. Although the raw recorded camera image is a low-contrast, random and seemingly information-less image (Fig. 1b), its autocorrelation (Fig. 1c) is essentially identical to the object's autocorrelation, as if it had been imaged by an aberration-free diffraction-limited optical system that had replaced the scattering medium (Fig. 1e–g). The object's image is obtained from its autocorrelation by an iterative phase-retrieval algorithm[27,30,35,36] (Fig. 1d).

The reason why the autocorrelation of the diffused light is essentially identical to the object's autocorrelation is the intrinsic isoplanatism that arises from the angular 'memory effect' for speckle correlation[32–34]. Simply put, the memory effect states that light

[1]Institut Langevin, UMR7587 ESPCI ParisTech and CNRS, INSERM ERL U979, 1 Rue Jussieu, 75005 Paris, France, [2]Laboratoire Kastler Brossel, Université Pierre et Marie Curie, Ecole Normale Supérieure, CNRS, Collège de France, 24 rue Lhomond, 75005 Paris, France. *e-mail: ori.katz@espci.fr

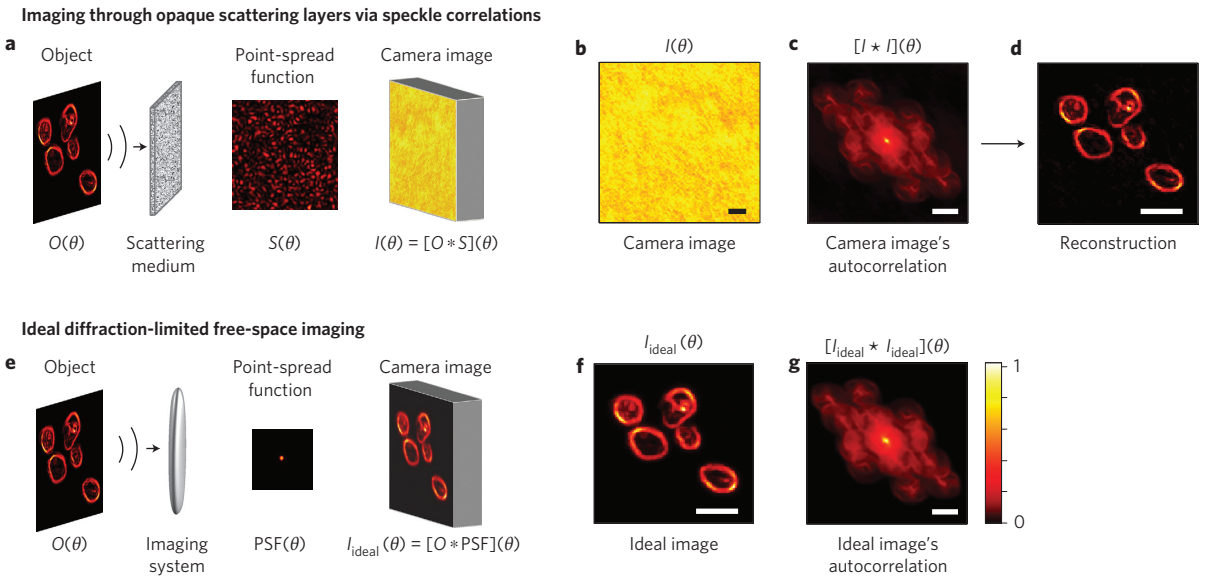

Figure 1 | Non-invasive imaging through strongly scattering layers by speckle correlations: concept and numerical example. a, Experimental set-up. An object (a group of organelles in the numerical example) is hidden behind a visually opaque scattering medium. The object is illuminated by a spatially incoherent narrowband source and a high-resolution camera records the scattered light pattern on the other side of the scattering medium. **b**, Raw camera image, $I(\theta)$. Within the memory-effect range[32], this image is given by a convolution of the object intensity pattern $O(\theta)$ with a random speckle pattern $S(\theta)$. **c**, The autocorrelation of the seemingly information-less raw camera image, $[I \star I](\theta)$, is essentially identical to the object's autocorrelation (**g**) as if it had been imaged by an aberration-free optical system replacing the scattering medium (**e**–**g**), as a result of the sharply peaked autocorrelation of the speckle pattern[27,29,30]. **d**, The object's image is obtained from the autocorrelation of **b** by an iterative phase-retrieval algorithm[27,36]. Scale bars: 30 camera pixels.

from nearby points on the object is scattered by the diffusive medium to produce highly correlated, but shifted, random speckle patterns on the camera (Fig. 1a). Points at the object plane that lie at a relative distance Δx that is within the memory-effect range ($\Delta x \ll u{\cdot}\lambda/\pi L$) generate nearly identical speckle patterns on the camera. These patterns are shifted with respect to one another on the camera plane by a distance $\Delta y = \Delta x{\cdot}v/u$ (refs 18,34). For spatially incoherent illumination (as well as for fluorescence emission) no interference takes place between the different patterns and the camera image is simply a superposition of these identical shifted speckle intensity patterns, $S(\theta)$ and $S(\theta + \Delta\theta)$, where $\Delta\theta = \Delta x/u$ is the viewing angle. This therefore allows the system of Fig. 1a to be viewed as an incoherent imaging system with a shift-invariant point-spread function (PSF) that is equal to this random speckle pattern, $S(\theta)$, and with a magnification of $M = v/u$. The camera image, $I(y)$, is then given by a convolution of the object intensity pattern $O(x)$ with this PSF: $I(v\theta) = O(u\theta) * S(\theta)$—where the symbol $*$ denotes a convolution operation. Taking the autocorrelation of the camera image and using the convolution theorem yields[27,29,30]

$$[I \star I](\theta) = [(O * S) \star (O * S)](\theta) = [(O \star O) * (S \star S)](\theta) \quad (1)$$

where ★ denotes the autocorrelation operation. As the autocorrelation of the speckle pattern, $(S \star S)$, is a sharply peaked function[1,27,29] (essentially the autocorrelation of broadband noise), the right-hand side of equation (1) is effectively equal to the autocorrelation of the object's image $[O \star O](\theta)$. More precisely, the autocorrelation of the camera image is equal to the autocorrelation of the object as it would have been imaged by an aberration-free imaging system replacing the scattering medium[29] (Fig. 1e–g), with an additional constant background term C, which originates from the 2:1 peak-to-background ratio of the speckle autocorrelation (Supplementary Fig. 4):

$$[I \star I](\theta) = [I_{\text{ideal}} \star I_{\text{ideal}}](\theta) + C \quad (2)$$

The object's diffraction-limited image $I_{\text{ideal}}(\theta)$ can then be obtained from its autocorrelation using a Fienup-type iterative phase-retrieval algorithm[27,30,35] (Fig. 1d, see Methods). The result of this procedure is that the opaque layer effectively serves as a perfect thin lens. This is reminiscent of the results obtained with wavefront-controlled 'scattering lenses'[15,18] and the cross-correlation approach of Freund[34]. However, a major advantage of the presented technique is that, unlike these approaches, it does not require a long invasive calibration procedure involving an implanted detector[18] or a guide-star[15] to map the exact scattering properties of the sample. The exact scattering properties of the medium remain unknown and the imaging process is insensitive to changes in the microstructure of the medium.

Here, similar to stellar speckle interferometry[29–31] and the speckle scanning technique of Bertolotti *et al.*[27], the object image is recovered from its autocorrelation. However, in the present technique the autocorrelation of the object is retrieved from a single image, captured in a fraction of a second, eliminating the requirement for temporal averaging over multiple images of stellar speckle interferometry and the lengthy high-resolution angular scanning of Bertolotti's approach. This breakthrough is made possible by exploiting the ergodic-like property of speckle in the diffusive regime[34] and the very high pixel count of modern digital cameras. These allow one to recover the object's autocorrelation with high fidelity by spatially averaging the correlation function over the millions of speckle spots that are captured in a single image, rather than performing temporal ensemble averaging over multiple exposures[29]. In fact, every camera pixel effectively plays the role of a single illumination angle in the speckle-scanning technique of Bertolotti *et al.*[27], parallelizing the acquisition process a million-fold.

The limit on the angular field of view (FOV) of our technique is given in the diffusive regime by the memory effect range[32], estimated by its half width at half maximum angle, $\Delta\theta_{\text{FOV}} \approx \lambda/\pi L$. This is inversely proportional to the medium's thickness L and is, in theory, unlimited for a scattering surface of 'zero' thickness. An additional limiting factor is the finite aperture on the scattering

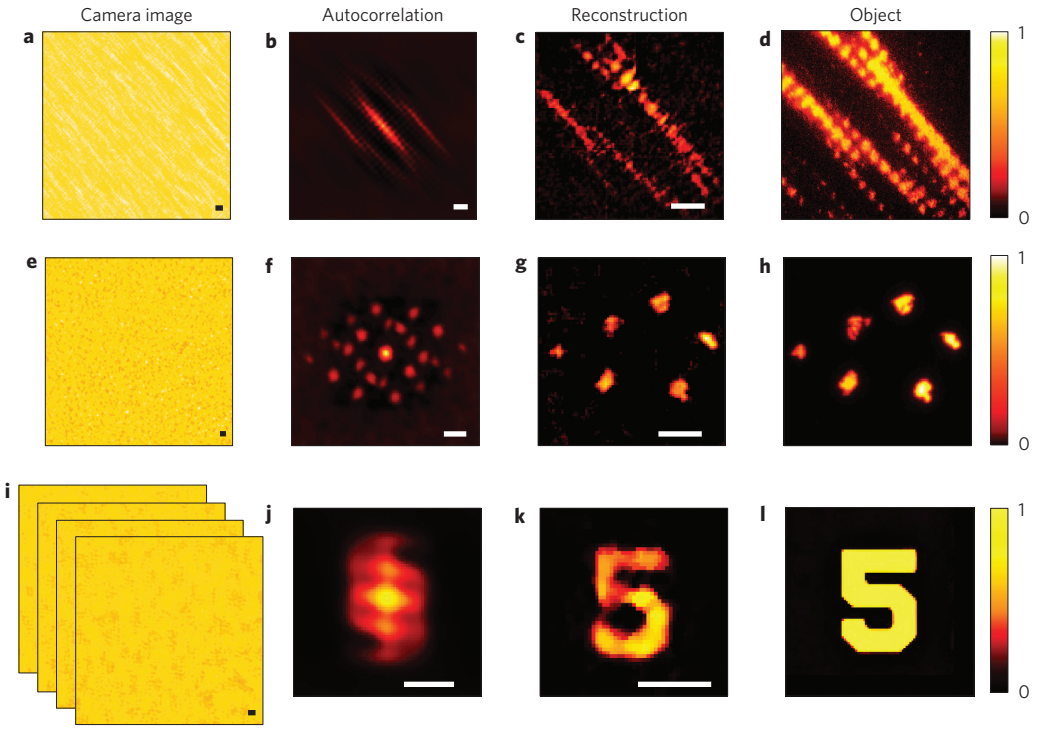

Figure 2 | Experimental imaging through a visually opaque optical diffuser and two biological samples. a, The raw, seemingly random, camera image of the scattered light (central part is shown). **b**, Corresponding autocorrelation of the camera image, revealing clear distinctive patterns. **c**, Object reconstructed from the autocorrelation of **b** by phase-retrieval. **d**, Object as imaged directly without the scattering medium. **e**–**l**, As in **a**–**d** for different imaged objects and scattering media: ~300-μm-thick chicken breast tissue (**e**–**h**); a fresh slice of 80-μm-thick shallot skin (**i**–**l**). In **i**–**l** the autocorrelation was ensemble-averaged from ten images taken at different times through the dynamic sample (Supplementary Movie 1). Scale bars: 20 camera pixels, corresponding to 200 μm at the object plane of (**a**–**c**), 700 μm (**e**–**g**) and 450 μm (**i**–**k**).

medium from which the light is collected, which will cause vignetting and decorrelation between points that illuminate a different portion of it. The effective 'entrance pupil' diameter D is dictated by the illuminated area on the scattering medium, as well as the effective diameter of any aperture stop placed between the scattering medium and the camera. This finite aperture also sets the angular imaging resolution, which is given by the diffraction limit[16,34], $\delta\theta \approx \lambda/nD$, where n is the refractive index behind the scattering layer.

Imaging through visually opaque samples

As a first experimental demonstration we imaged various objects through a scattering, visually opaque optical diffuser (Fig. 2a–d) and through two turbid biological samples (Fig. 2e–l). In these experiments the objects to be imaged were placed at distances of 10–60 cm behind the scattering sample and were back-illuminated by a narrowband spatially incoherent pseudothermal source (composed of a continuous-wave (c.w.) laser and rotating diffuser, Supplementary Fig. 1). The image of the scattered light was recorded by a 5 megapixel scientific complementary metal–oxide–semiconductor camera. The results of these experiments are summarized in Fig. 2. The leftmost column displays the central part of the raw camera images, which are low-contrast and seemingly random patterns, with no visible relation to the true shape of the imaged objects. However, the autocorrelations of these images reveal clear distinctive patterns (the second column from the left in Fig. 2). The hidden object's shape is recovered from this autocorrelation with high fidelity by phase retrieval[35] (see Methods). We demonstrate the reconstruction using several objects of various shapes and complexities, with different contrast of the raw camera images.

As only a single camera shot is required, the technique can be used to image through dynamically varying samples, such as the freshly cut shallot sample of Fig. 2i–l (Supplementary Fig. 6). Interestingly, the dynamics of the sample can be exploited to yield a better estimate of the autocorrelation, by acquiring a set of images of the scattered light at different times (Fig. 2i, Supplementary Movie 1). Although the hidden object could be reconstructed from any single image of this set, averaging the autocorrelation over all ten acquired images yields a better estimate for the autocorrelation due to ensemble averaging over different speckle realizations, exactly as is done in stellar speckle interferometry[29,30]. The dynamics of natural samples can thus be exploited, rather than fought against, to image hidden objects.

Figure 3 presents the results of a complementary non-invasive imaging experiment, where the target objects are hidden between two visually opaque diffusers. The objects are illuminated through the first diffuser and the image of the scattered light that has passed through the object is recorded through the second diffuser. Again, the true image of the object is reconstructed with high fidelity from the scattered light pattern (Fig. 3c,g). In contrast, only a blurred diffuse halo can be obtained conventionally when imaging through either of the two enclosing diffusers (Fig. 3b,e,f,i), as would be the case, for example, when attempting to image through a scattering eggshell.

An interesting feature of the presented technique is its infinite depth of field. A planar object will always be imaged with a diffraction-limited resolution, regardless of its distance from the scattering layer. The reason for this is that the PSF of the scattered light is always a speckle pattern with a sharply peaked autocorrelation function. In contrast, a conventional lens-based system's PSF has a diffraction-limited autocorrelation peak only within a small axial range. An experimental demonstration of this feature is presented in Supplementary Fig. 2. The extended depth of field is obtained for the same reason as in wavefront coding

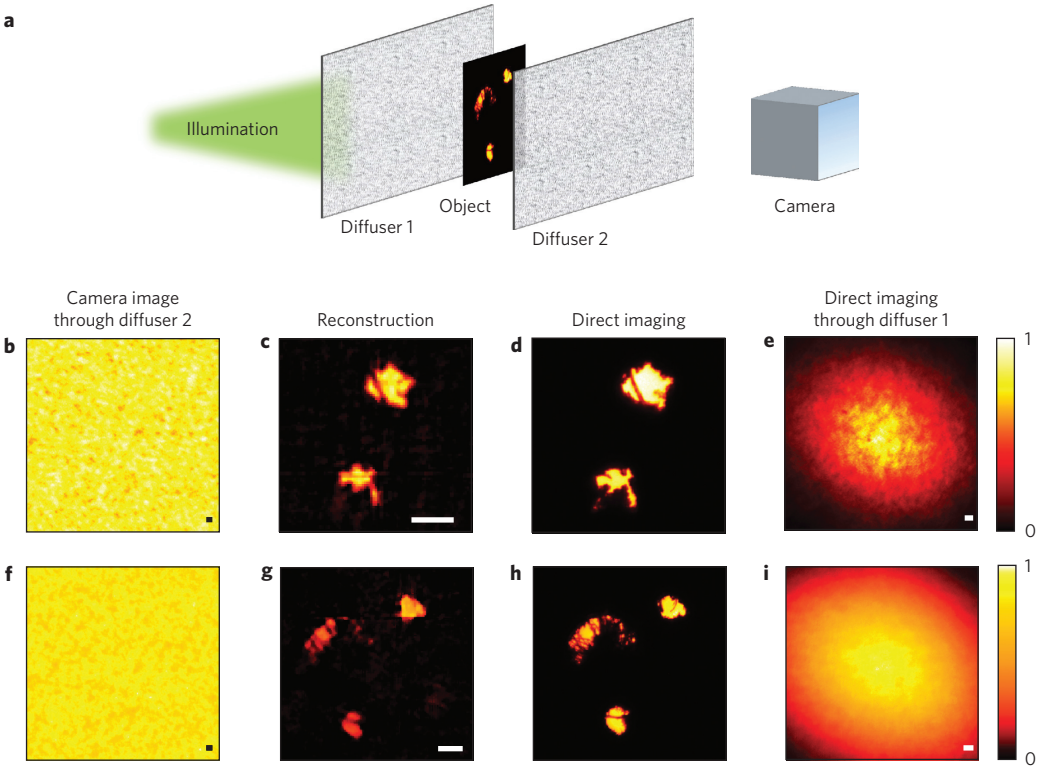

Figure 3 | Non-invasive imaging of objects enclosed between two diffusers. a, Sketch of the experiment (Supplementary Fig. 1b). The object is placed between two visually opaque diffusers (at distances of 20 mm and 18.5 cm, respectively). The object is illuminated through the first diffuser and the scattered light pattern is observed through the second diffuser. **b**, Raw camera image of the scattered light (central part shown). **c**, Reconstructed image from the autocorrelation of **b**. **d**, Object as imaged directly without any diffusers. **e**, Conventional imaging of the object through diffuser 1 (the object is back-illuminated). **f**–**i**, As in **b**–**e** for a different object. Scale bars: 20 camera pixels, corresponding to 270 μm at the object plane.

techniques[37,38]; the scattering medium is, in essence, a random wavefront coder.

Imaging 'around corners'

The presented technique can also work in reflection; that is, it can be applied to the imaging of occluded objects 'around the corner' using the light back-scattered from a diffusive wall. An experimental demonstration of imaging using a single image of the diffuse back-scattered light is presented in Fig. 4. The scattering sample in this experiment is a thick layer of ZnO powder, which is essentially white paint. The imaging resolution and FOV in reflection are given by the same expressions as for transmission geometry but by replacing the medium thickness L with the transport mean-free-path l^* (ref. 34). Remarkably, the stronger the scattering (shorter mean-free-path), the larger the FOV. For highly scattering white paint pigments l^* is on the order of 1 μm (refs 8,39), corresponding to an angular FOV exceeding several degrees. Here, using only a standard camera, the scattering wall effectively serves as a mirror. This is a significant simplification over previous 'around the corner' imaging approaches[18,40].

Seeing through a scattering layer with a camera-phone

As a final demonstration of the simplicity and applicability of the presented technique we show that the requirements for implementing it (see Discussion) can be satisfied using consumer-grade handheld cameras, as are available to millions today. To this end we repeated the experiments of Fig. 2 using a Nokia Lumia 1020 smartphone, which has a 41 megapixel sensor. We placed various objects 20 cm from the diffuser and simply took an image of the scattered light with the camera-phone, which was placed on the other side of the diffuser (Fig. 5a,b). We retrieve the hidden objects from a single scattered light image, taken at 1/100 to 1/20 s exposure times (Fig. 5c–g).

The major hurdles that should be considered when using such low-cost imaging devices for these experiments are their fixed miniature optics, which dictate the viewing angle and magnification, and possibly introduce aberrations that limit the FOV. In addition, the Bayer colour filter sensor array introduces pixel-scale artefacts when interpolated to the full resolution. Finally, when processing images saved with the common JPEG compression and gamma correction, additional artefacts and dynamic range limitations interfere with the reconstruction. However, these still allow the reconstruction of simple objects, as we demonstrate in Fig. 5g (in Fig. 5c–f, images were captured in a linear 'digital RAW' format, see Methods).

Discussion

Several conditions should be met in order to allow high-fidelity imaging with the presented technique. First, the object's angular dimensions, as seen through the random medium, must be smaller than the memory-effect range (the FOV). In addition, the object's axial dimensions should not extend beyond a distance of $\delta z = (2\lambda/\pi)(u/D)^2$, which is the axial decorrelation length of the speckled PSF[34]. Parts of the object that lie beyond these ranges would produce uncorrelated speckle patterns and would not contribute properly to the calculated autocorrelation[28]. As a result, similar to other memory-effect-based techniques[15,18,27] the approach is effective when the object's distance from the scattering layer is considerably larger than the effective layer thickness. Potential applications include imaging in an eggshell geometry, where the scattering originates predominantly from a thin enclosing layer, LIDAR imaging through thin scattering layers, and imaging around corners. Wide-field imaging inside thick, multiply-scattering tissue

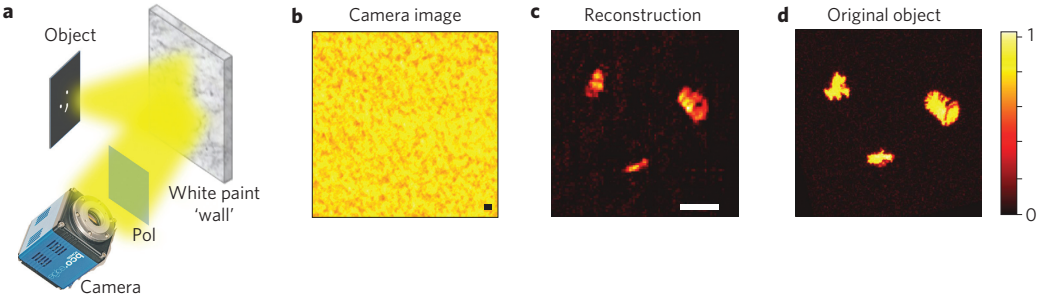

Figure 4 | Single-shot imaging 'around corners' using back-scattered light. a, Light from a spatially incoherent illuminated object hits a highly scattering layer of ZnO 'white paint'. A single image of the backscattered diffused light pattern at a given polarization is recorded by a high-resolution camera. **b**, Central part of the raw camera image. **c**, Reconstructed object's image from autocorrelation of the camera image. **d**, The real hidden object's image. Scale bars: 20 camera pixels, corresponding to 400 μm at the object plane. Pol, linear polarizer.

still presents a challenge. Interestingly, experimental characterization of the memory-effect range for a 0.5-mm-thick chicken breast tissue (Supplementary Fig. 8) gives a considerably larger angular FOV than that expected in the diffusive regime. This is an encouraging result for applying the technique at shallow imaging depths. Second, a single speckle grain should be well resolved by the camera (adequate Shannon–Nyquist sampling); that is, the speckle grain should be twice as large as the camera pixel size. This condition is easily met by adjusting the distance of the camera from the scattering medium and/or by placing an appropriate aperture stop behind the scattering medium (Supplementary Fig. 1). Third, to obtain a large number of resolved resolution cells at the object plane ($B = (\Delta\theta_{FOV}/\delta\theta)^2 \propto (D/L)^2$), the available aperture diameter on the scattering medium, D, should be considerably larger than the effective medium thickness: $D \gg L$. A practical limit on increasing the resolution is the resulting reduced raw image contrast, due to the increased number of bright resolution cells on the object (N, the number of summed shifted speckle patterns). The practical limit on N is the camera's full well capacity (Supplementary Section 3). As a consequence, the technique would generally perform better in dark-field illumination and with sparsely tagged objects (as found, for example, in photo-activated localization microscopy[41]) rather than in bright-field imaging scenarios. Fourth, to maximize the raw image contrast, the spectral bandwidth used to form the image should be narrower than the speckle spectral correlation width, $\delta\omega$ (refs 18,34,42) (taking into account the geometrical propagation after the sample[30,43]), such that the PSF, $S(\theta)$, is indeed a high-contrast speckle pattern (Supplementary Fig. 5). In other words, for a maximum raw image contrast, the detected light temporal coherence should exceed the optical delay spread of the light's diffusion through the medium, Δt, and the additional geometrical path length differences before and after the sample[30,43]. In the diffusive regime (that is, for $L \gg l^*$), $\Delta t_t \approx 2\pi L^2/cl^*$ in transmission and $\Delta t_r \approx 2\pi l^*/c$ in reflection[34]. For example, for highly scattering white-paint pigments such as the one used in reflection in Fig. 4 ($l^* \approx 2$ μm; ref. 39) this corresponds to $\Delta t_r \approx 40$ fs, that is, a decorrelation bandwidth of ~20 nm in reflection in the visible range. For transmission through soft tissues where l^* is on the order of 0.5–1 mm (refs 2,44), the above expression for Δt_t is valid only for samples that are considerably thicker than 1 mm. Experimental measurements for a ~500-μm-thick chicken breast sample, such as the one used in Fig. 2e, give a sample decorrelation bandwidth exceeding 10 nm (Supplementary Fig. 7). The requirement for a limited detected spectral width can be easily met by either controlling the illumination bandwidth as was done here, or by placing a narrowband filter in front of the camera when temporally incoherent signals, such as fluorescence, are used. The latter is routinely performed in stellar speckle interferometry using natural light[30] and was also demonstrated recently with broadband white light scattered by an optical diffuser[18] and with fluorescent emission from an object buried in 0.5-mm-thick scattering biological tissue[45]. It is important to note that it is not imperative to filter the light to a bandwidth smaller than $\delta\omega$ and that using a larger bandwidth is possible. This would lower the raw image contrast, but should not affect the imaging resolution as the autocorrelation of $S(\theta)$ remains a sharply peaked function (Supplementary Fig. 5). Alternatively, several spectral bands could be processed simultaneously by separating them to several cameras, allowing additional ensemble averaging or multispectral imaging. Due to the limited usable bandwidth, attractive forms of contrast are those where the spectral bandwidth is inherently narrow. These include transmission and reflection (for example, as in LIDAR), Raman and ultrasound-encoded (acousto-optical) imaging[46]. The usable bandwidth limits the signal collection efficiency when broadband fluorescence is considered, a limitation that does not exist in the approach of Bertolotti and colleagues[27].

The final condition is that the number of sampled and processed speckle grains should be maximized. As in other digital speckle correlation techniques, an inherent source of noise originates from replacing the ensemble averaging with averaging over a finite number of speckles (ultimately limited by the number of camera pixels)[47]. This is important for both accurately estimating the autocorrelation function as well as for correctly subtracting its background. In the present experiments, by using multi-megapixel sensor arrays we were able to obtain a satisfactory signal-to-noise ratio (SNR) by processing $\sim 1 \times 10^6$ speckle grains in a single camera shot. For a thorough analysis of this and other sources of noise in speckle interferometry, we refer the reader to the works of Dainty[30,31].

In this proof of concept we have used Fienup's basic phase-retrieval algorithms[27,35] and have made no special effort to overcome the common stagnation and artefact issues of these simple algorithms[36]. Higher-fidelity reconstruction is anticipated by applying more advanced methods, such as the majority voting and reduced support constraint[36]. Furthermore, by using different speckle interferometry analysis techniques[30,36], such as triple-correlation analysis[31], additional phase information may be obtained from the available data in some cases. Another potential improvement may be achieved by applying compressive phase-retrieval algorithms[48,49] to reduce the acquisition time and increase the reconstruction fidelity. In particular, such improvement would be required in scenarios involving complex objects and low-SNR conditions, where the high-intensity features of the objects tend to dominate the reconstruction[27]. Interestingly, if one is only interested in tracking unknown objects without reconstructing their shape, a simple cross-correlation between images taken at different times can be performed, without requiring any phase-retrieval algorithm.

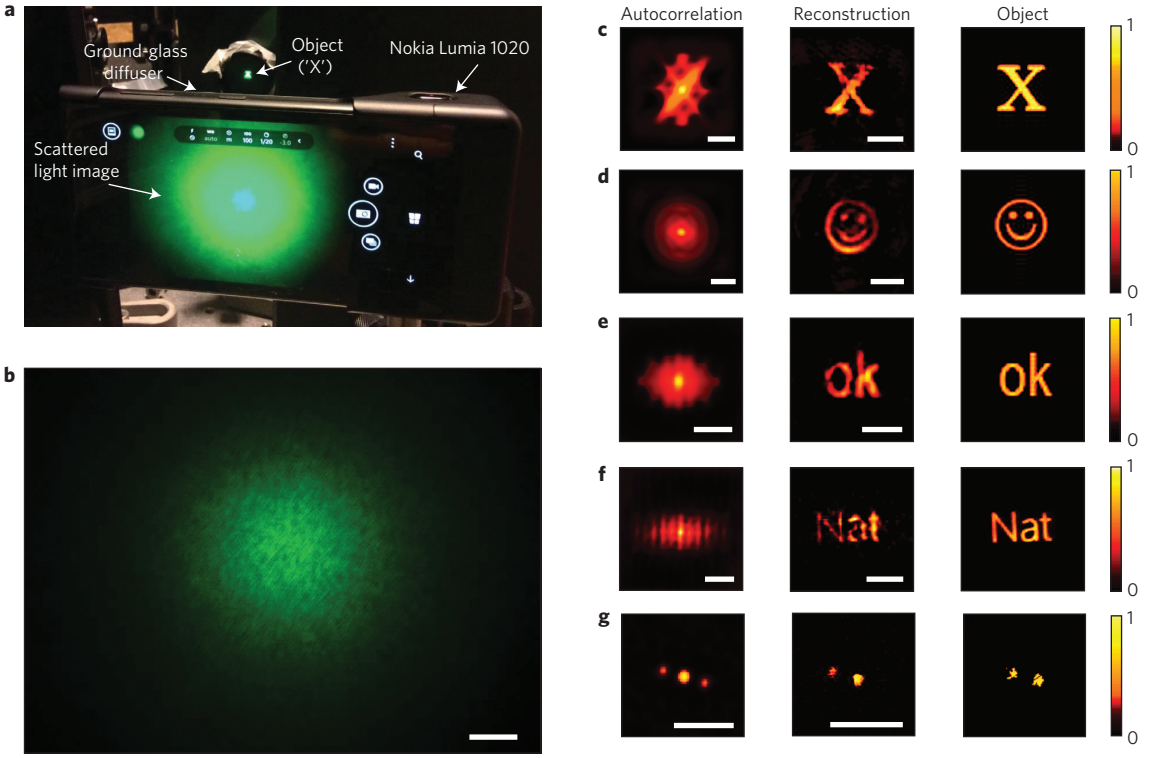

Figure 5 | Imaging through a visually opaque layer with a camera-phone. a, Photograph of the experiment: a camera-phone (Nokia Lumia 1020) is used to take a picture of the object (the letter 'X', in this image) through a highly scattering ground-glass diffuser. **b**, Raw camera image in a linear intensity scale (scale bar: 500 pixels). **c**, Left column: calculated autocorrelation of the image in **b**. Middle column: reconstructed object from the image autocorrelation. Right column: image of the real hidden object. **d**–**g**, As in **c** but for different objects. In **g**, a nonlinear gamma-corrected JPEG image was processed. Scale bars: 50 camera pixels, corresponding to 1.7 mm at the object plane.

We have shown that an unknown random medium can serve as part of the imaging device and that multiply-scattered light can be used rather than filtered out to form an image. This is closely related to the well-studied technique of time-reversal[7,50], which has found applications in acoustics[50], radiofrequency (RF) communication and seismology. A related interesting link concerns passive correlation-based imaging[51], where temporal correlations of broadband signals are analysed. Similar to these techniques, our technique is lensless (the scattering medium effectively serves as the lens) and, as such, it may find applications in other spectral or wave-propagation domains where fabrication of lenses is a challenge. As the memory effect only dictates the FOV angular range, the presented millimetre-scale experiments can, in principle, be scaled to micrometre- or metre-scale scenarios.

Methods

Experimental set-up. The complete experimental set-ups for imaging in transmission and reflection are presented in Supplementary Fig. 1. The imaged objects were printed transparencies, a United States Air Force resolution target (Thorlabs R3L3S1N) and groups of holes of various shapes made on a black screen. The objects were illuminated by a narrow bandwidth spatially incoherent pseudothermal source at a wavelength of 532 nm, based on a Coherent Compass 215M-50 c.w. laser. The light collection aperture diameter on the scattering media was limited to 0.5–1 cm by a variable iris. The camera used in the experiments of Figs 2–4 is a PCO edge 5.5 (2,560 × 2,160 pixels). The camera integration time in the different experiments was 10 ms to 2 s (typically a few hundred milliseconds).

The objects were placed at distances of 20–60 cm from the scattering sample and the camera was placed at distances of 9–15 cm from the medium. In the experiments of Fig. 5, the light collection aperture was limited to ~0.9 mm and the camera-phone was placed as close as possible to the diffuser (~1 mm distance). The diffuser was a 220 grit-ground-glass diffuser (DG10-220-MD Thorlabs). The second diffuser that enclosed the object from the illumination side in Fig. 3 was a 10° light shaping diffuser (Newport). The ZnO sample was made by sedimentation comprising vertical deposition and subsequent drying of a water suspension of ZnO powder (Zinc-Oxide 205532, Sigma-Aldrich). The chicken breast and shallot samples were placed between two microscope glass slides, which were held vertically. The characterization of the properties of the biological samples is provided in Supplementary Section 6. The ground glass diffuser memory-effect range was characterized by Bertolotti *et al.*[27] and the ZnO sample transport mean free path was characterized by Curry and co-authors[39].

For the camera-phone imaging experiment of Fig. 5, the only modification to the smartphone camera was the reduction of its entrance aperture so that the individual speckle grains were resolved by more than two camera pixels (see Discussion). This was done by simply placing a black screen with a ~0.9-mm-diameter pinhole on top of the camera lens.

Image processing. The raw camera image was spatially normalized for the slowly varying envelope of the scattered light pattern halo by dividing the raw camera image by a low-pass-filtered version of it. The normalized image was smoothed by a Gaussian kernel with a standard-deviation width of 0.5–2 pixels. The autocorrelation of the processed image was calculated by an inverse Fourier transform of its energy spectrum (effective periodic boundary conditions). In the experiments of Fig. 4 the autocorrelation was calculated directly from the central 1,200 × 1,200 pixels of the raw camera image, without correcting for the scattered light envelope.

The resulting autocorrelation was cropped to a rectangular window with dimensions ranging between 100 × 100 pixels and 320 × 320 pixels (depending on the imaged object dimensions), and the minimum pixel brightness in this window was background-subtracted from the entire autocorrelation trace. In the experiments of Fig. 5, a two-dimensional Tukey window was applied on the autocorrelation before applying the phase-retrieval reconstruction algorithm.

In the camera-phone experiments of Fig. 5a–f, the full 38 megapixel resolution raw images (5,360 × 7,152 pixels) were saved in a digital negative (DNG) RAW format and the green channel was converted to a bitmap format using the DCRaw plug-in for ImageJ. The conversion was done in a 16 bit linear scale, with a 'Variable Number of Gradient' interpolation method. The converted monochrome image was used to calculate the autocorrelation as detailed above. In the experiment of Fig. 5g the green channel from a full-resolution JPEG format was used.

Phase-retrieval algorithm. The phase-retrieval algorithm was implemented according to the recipe provided by Bertolotti and co-authors[27] (for details see Supplementary Section 7). The object constraints used were it being real and non-negative. The algorithms were implemented in Matlab and run on an NVIDIA GeForce GTX 670 graphics processing unit (GPU) with 1,344 cores, using the

gpuarray function. A single run of the algorithm (composed of 2,000 iterations) on this GPU took between 1 s and 2 s. The displayed reconstructed images of Figs 5, 2k and 3 are the reconstruction results after median-filtering with a rectangular 3×3 pixel kernel.

Received 17 March 2014; accepted 16 July 2014; published online 31 August 2014

References

1. Goodman, J. W. *Speckle Phenomena in Optics: Theory and Applications* (Roberts & Co., 2007).
2. Ntziachristos, V. Going deeper than microscopy: the optical imaging frontier in biology. *Nature Methods* **7,** 603–614 (2010).
3. Goodman, J. W., Huntley Jr, W. H., Jackson, D. W. & Lehmann, M. Wavefront-reconstruction imaging through random media. *Appl. Phys. Lett.* **8,** 311–313 (1966).
4. Kogelnik, H. & Pennington, K. S. Holographic imaging through a random medium. *J. Opt. Soc. Am.* **58,** 273–274 (1968).
5. Tyson, R. K. *Principles of Adaptive Optics* 3rd edn (Academic, 2010).
6. Débarre, D. *et al.* Image-based adaptive optics for two-photon microscopy. *Opt. Lett.* **34,** 2495–2497 (2009).
7. Mosk, A. P., Lagendijk, A., Lerosey, G. & Fink, M. Controlling waves in space and time for imaging and focusing in complex media. *Nature Photon.* **6,** 283–292 (2012).
8. Vellekoop, I. M. & Mosk, A. P. Focusing coherent light through opaque strongly scattering media. *Opt. Lett.* **32,** 2309–2311 (2007).
9. Popoff, S. M. *et al.* Measuring the transmission matrix in optics: an approach to the study and control of light propagation in disordered media. *Phys. Rev. Lett.* **104,** 100601 (2010).
10. Cizmar, T., Mazilu, M. & Dholakia, K. *In situ* wavefront correction and its application to micromanipulation. *Nature Photon.* **4,** 388–394 (2010).
11. Katz, O., Small, E., Bromberg, Y. & Silberberg, Y. Focusing and compression of ultrashort pulses through scattering media. *Nature Photon.* **5,** 372–377 (2011).
12. Aulbach, J., Gjonaj, B., Johnson, P. M., Mosk, A. P. & Lagendijk, A. Control of light transmission through opaque scattering media in space and time. *Phys. Rev. Lett.* **106,** 103901 (2011).
13. Popoff, S., Lerosey, G., Fink, M., Boccara, A. C. & Gigan, S. Image transmission through an opaque material. *Nature Commun.* **1,** 81 (2010).
14. Conkey, D. B., Caravaca-Aguirre, A. M. & Piestun, R. High-speed scattering medium characterization with application to focusing light through turbid media. *Opt. Express* **20,** 1733–1740 (2012).
15. Vellekoop, I. M. & Aegerter, C. M. Scattered light fluorescence microscopy: imaging through turbid layers. *Opt. Lett.* **35,** 1245–1247 (2010).
16. Vellekoop, I. M., Lagendijk, A. & Mosk, A. P. Exploiting disorder for perfect focusing. *Nature Photon.* **4,** 320–322 (2010).
17. Hsieh, C.-L., Pu, Y., Grange, R., Laporte, G. & Psaltis, D. Imaging through turbid layers by scanning the phase conjugated second harmonic radiation from a nanoparticle. *Opt. Express* **18,** 20723–20731 (2010).
18. Katz, O., Small, E. & Silberberg, Y. Looking around corners and through thin turbid layers in real time with scattered incoherent light. *Nature Photon.* **6,** 549–553 (2012).
19. He, H., Guan, Y. & Zhou, J. Image restoration through thin turbid layers by correlation with a known object. *Opt. Express* **21,** 12539–12545 (2013).
20. Xu, X., Liu, H. & Wang, L. V. Time-reversed ultrasonically encoded optical focusing into scattering media. *Nature Photon.* **5,** 154–157 (2011).
21. Si, K., Fiolka, R. & Cui, M. Fluorescence imaging beyond the ballistic regime by ultrasound-pulse-guided digital phase conjugation. *Nature Photon.* **6,** 657–661 (2012).
22. Wang, Y. M., Judkewitz, B., DiMarzio, C. A. & Yang, C. Deep-tissue focal fluorescence imaging with digitally time-reversed ultrasound-encoded light. *Nature Commun.* **3,** 928 (2012).
23. Kong, F. *et al.* Photoacoustic-guided convergence of light through optically diffusive media. *Opt. Lett.* **36,** 2053–2055 (2011).
24. Judkewitz, B., Wang, Y. M., Horstmeyer, R., Mathy, A. & Yang, C. Speckle-scale focusing in the diffusive regime with time reversal of variance-encoded light (TROVE). *Nature Photon.* **7,** 300–305 (2013).
25. Chaigne, T. *et al.* Controlling light in scattering media non-invasively using the photoacoustic transmission matrix. *Nature Photon.* **8,** 58–64 (2014).
26. Tang, J., Germain, R. N. & Cui, M. Superpenetration optical microscopy by iterative multiphoton adaptive compensation technique. *Proc. Natl Acad. Sci. USA* **109,** 8434–8439 (2012).
27. Bertolotti, J. *et al.* Non-invasive imaging through opaque scattering layers. *Nature* **491,** 232–234 (2012).
28. Yang, X., Pu, Y. & Psaltis, D. Imaging blood cells through scattering biological tissue using speckle scanning microscopy. *Opt. Express* **22,** 3405–3413 (2014).
29. Labeyrie, A. Attainment of diffraction limited resolution in large telescopes by Fourier analysing speckle patterns in star images. *Astron. Astrophys.* **6,** 85–87 (1970).
30. Dainty, J. C. *Laser Speckle and Related Phenomena* (Springer, 1984).
31. Ayers, G., Northcott, M. & Dainty, J. Knox–Thompson and triple-correlation imaging through atmospheric turbulence. *J. Opt. Soc. Am. A* **5,** 963–985 (1988).
32. Freund, I., Rosenbluh, M. & Feng, S. Memory effects in propagation of optical waves through disordered media. *Phys. Rev. Lett.* **61,** 2328–2331 (1988).
33. Feng, S., Kane, C., Lee, P. A. & Stone, A. D. Correlations and fluctuations of coherent wave transmission through disordered media. *Phys. Rev. Lett.* **61,** 834–837 (1988).
34. Freund, I. Looking through walls and around corners. *Phys. A* **168,** 49–65 (1990).
35. Fienup, J. R. Phase retrieval algorithms: a comparison. *Appl. Opt.* **21,** 2758–2769 (1982).
36. Fienup, C. D. J. in *Image Recovery: Theory and Application* (ed. Stark, H.) 231–275 (Academic, 1987).
37. Dowski, J. E. R. & Cathey, W. T. Extended depth of field through wave-front coding. *Appl. Opt.* **34,** 1859–1866 (1995).
38. Cathey, W. T. & Dowski, E. R. New paradigm for imaging systems. *Appl. Opt.* **41,** 6080–6092 (2002).
39. Curry, N. *et al.* Direct determination of diffusion properties of random media from speckle contrast. *Opt. Lett.* **36,** 3332–3334 (2011).
40. Velten, A. *et al.* Recovering three-dimensional shape around a corner using ultrafast time-of-flight imaging. *Nature Commun.* **3,** 745 (2012).
41. Betzig, E. *et al.* Imaging intracellular fluorescent proteins at nanometer resolution. *Science* **313,** 1642–1645 (2006).
42. Van Beijnum, F., van Putten, E. G., Lagendijk, A. & Mosk, A. P. Frequency bandwidth of light focused through turbid media. *Opt. Lett.* **36,** 373–375 (2011).
43. Small, E., Katz, O. & Silberberg, Y. Spatiotemporal focusing through a thin scattering layer. *Opt. Express* **20,** 5189–5195 (2012).
44. Cheong, W.-F., Prahl, S. A. & Welch, A. J. A review of the optical properties of biological tissues. *IEEE J. Quantum Electron.* **26,** 2166–2185 (1990).
45. Vellekoop, I. M., Cui, M. & Yang, C. Digital optical phase conjugation of fluorescence in turbid tissue. *Appl. Phys. Lett.* **101,** 081108 (2012).
46. Elson, D. S., Li, R., Dunsby, C., Eckersley, R. & Tang, M.-X. Ultrasound-mediated optical tomography: a review of current methods. *Interface Focus* **1,** 632–648 (2011).
47. Skipetrov, S. E. *et al.* Noise in laser speckle correlation and imaging techniques. *Opt. Express* **18,** 14519–14534 (2010).
48. Moravec, M. L., Romberg, J. K. & Baraniuk, R. G. Wavelets XII. *Proc. SPIE* **6701,** 670120 (2007).
49. Shechtman, Y., Beck, A. & Eldar, Y. GESPAR: Efficient phase retrieval of sparse signals. *IEEE Trans. Signal Process.* **62,** 928–938 (2014).
50. Fink, M. Time reversed acoustics. *Phys. Today* **50,** 34–40 (March, 1997).
51. Weaver, R. L. & Lobkis, O. I. Ultrasonics without a source: thermal fluctuation correlations at MHz frequencies. *Phys. Rev. Lett.* **87,** 134301 (2001).

Acknowledgements

The authors thank D. Martina and A. Liutkus for help with the GPU implementation of the algorithm, P. Ducellier for the Nokia Lumia 1020 camera-phone, J. Bertolotti for discussions and D. Andreoli for the spectral decorrelation measurements. This work was funded by the European Research Council (grant no. 278025). O.K. was supported by the Marie Curie Intra-European fellowship for career development (IEF) and a Rothschild fellowship.

Author contributions

O.K. conceived the idea, performed the numerical simulations, wrote the reconstruction algorithm and designed the initial experiments. O.K., P.H. and S.G. discussed the experimental implementation. O.K. and P.H. performed the experiments and analysed the results. O.K, M.F. and S.G. discussed the results. O.K. wrote the manuscript with contributions from all authors.

Additional information

Supplementary information is available in the online version of the paper. Reprints and permissions information is available online at www.nature.com/reprints. Correspondence and requests for materials should be addressed to O.K.

Competing financial interests

The authors declare no competing financial interests.